

Structural origin of enhanced critical temperature in ultrafine multilayers of cuprate superconducting films

Fengshan Zheng,¹ Gennady Logvenov,² Ivan Bozovic,² Yimei Zhu,^{2,*} and Jiaqing He^{1,†}¹*Department of Physics, South University of Science and Technology of China, Shenzhen 518055, P. R. China*²*Condensed Matter Physics and Material Science Department, Brookhaven National Laboratory, Upton, New York 11973, USA*

(Received 12 February 2014; published 16 May 2014)

The interface layers of $\text{La}_{2-x}\text{Sr}_x\text{CuO}_4$ (LSCO) thin films epitaxially grown on LaSrAlO_4 substrates by molecular beam epitaxy were investigated using transmission electron microscopy (TEM). In single-phase LSCO film, we observed an irregular layering sequence near the interface between the film and the substrate, as well as an abundance of oxygen vacancies in CuO_2 layers. A multilayer LSCO film with a high critical temperature ($T_c = 44.5$ K) showed perfect interfaces between the sublayers. Furthermore, by combining scanning TEM, electron energy-loss spectroscopy, and electron holography, we show that there is little or no interdiffusion between the sublayers. The interfacial defects and oxygen vacancies reduce T_c , while the compressive strain in high-quality multilayers enhances T_c .

DOI: [10.1103/PhysRevB.89.184509](https://doi.org/10.1103/PhysRevB.89.184509)

PACS number(s): 74.78.-w, 68.37.Lp

I. INTRODUCTION

The $\text{La}_{2-x}\text{Sr}_x\text{CuO}_4$ (LSCO) family of compounds (solid solutions) has attracted much attention [1–23]; since with increasing the Sr doping level x , several quantum phase transitions occur as the system's ground state transits from an antiferromagnetic insulator to a high-temperature superconductor (HTS) and then to a nonsuperconducting metal. Much of the research has been focused on understanding this behavior as well as on improving the physical properties, in particular the critical temperature (T_c). One effective strategy has been to employ the epitaxial strain, which strongly affects the superconducting properties [4–9,18], e.g., compressive strain increases while tensile strain lowers T_c in LSCO. Significantly, the copper-apical-oxygen distance has been found to also increase with the compressive strain and decrease with tensile strain and, in fact, to scale linearly with T_c [24,25].

Another successful strategy has relied on artificial engineering of HTS multilayers and superlattices. For example, bilayer and multilayer LSCO films, where the constituent layers are insulating La_2CuO_4 and nonsuperconducting metallic LSCO (e.g., with $x = 0.45$), have shown T_c enhanced by as much as 25% compared to the optimized single-phase films, even though this interface superconductivity originated from HTS fluid confined to a single CuO_2 layer [12–16,19,26,27]. This interfacial enhancement has not been fully understood, although it was noticed that in such bilayer thin films there is an additional “Madelung strain”: Long-range electrostatic interactions cause the c axis lattice constant of the top layer to adjust to that of the bottom layer, and this correlates with the enhanced T_c of the film [13].

On the other hand, these paths to increase T_c are hindered by various technical problems. Interface superconductivity is vulnerable to many factors that can reduce T_c : interface roughness, cation interdiffusion, structure reconstruction caused by electrostatic incongruity between the two (ionic) materials, occurrence of cation or oxygen vacancies, intersite

substitutions, other structural defects, charge depletion or accumulation driven by the difference in chemical potentials, etc. [12–16,19].

Hence, for a full understanding of high- T_c interface superconductivity, atomically resolved measurements in chemical composition along the growth direction of the chemical composition (e.g., the Sr dopant concentration x) and the crystallographic structure need to be investigated in detail [18,19,28,29]. Here, we report our study of interfacial integrity and chemical composition of several LSCO films by means of advanced scanning/transmission electron microscopy (S/TEM) techniques, including imaging, electron energy-loss spectroscopy, and off-axis electron holography. The data provide an insight into the relationship between T_c and the interfacial atomistic structure: The enhanced T_c indeed correlates positively with the compressive strain, while interfacial defects and oxygen vacancies in the film can largely reduce T_c .

II. METHODS

For the present study, the LSCO samples were grown using atomic-layer-by-layer molecular beam epitaxy (ALL-MBE) [30,31]. For the substrate, we used LaSrAlO_4 (LSAO), which has the same space group and structure as LSCO but slightly different in-plane lattice parameters, providing a small compressive strain. For reference, a 30-nm-thick single-phase LSCO film (sample A in what follows) was grown first. Then we synthesized a multilayer film (sample B) of the same thickness film but consisting of six LSCO sublayers, each 5 nm thick, with varied Sr doping ($x = 0.35, 0.30, 0.25, 0.20, 0.15$, and 0.10), as illustrated schematically in the inset of Fig. 1. The critical temperature of sample B, measured by the ac susceptibility (mutual inductance) technique, was $T_c = 44.5$ K (see Fig. 1). (For comparison, in the best single-phase LSCO films grown under the same conditions, we had $T_c < 40$ K.) In the imaginary (dissipative, out-of-phase) channel of mutual inductance, we also notice four extra and small peaks close to the main big peak, suggestive of some small variations in the chemical composition. Investigations using

*zhu@bnl.gov

†he.jq@sustc.edu.cn

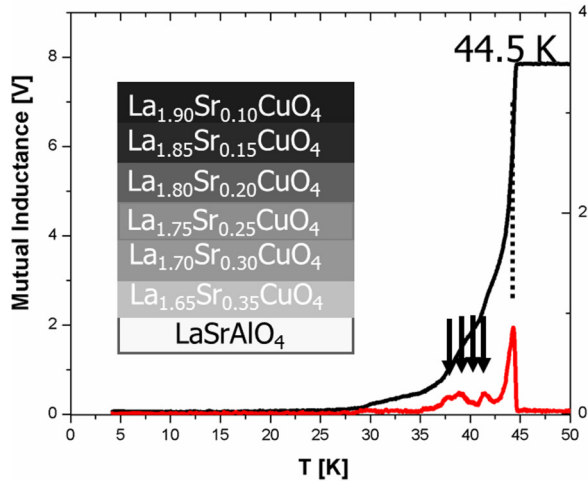


FIG. 1. (Color online) Temperature dependence of susceptibility, measured by the mutual inductance technique, of a multilayer LSCO film, showing a superconducting transition at 44.5 K.

TEM, including high resolution TEM (HRTEM), scanning TEM (STEM), electron energy loss spectroscopy (EELS), and electron holography, were carried out with JEOL-2100, double aberration corrected JEOL-2200CMO and probe-corrected Hitachi HD-2700 microscopes. High-resolution numerical simulations were carried out with the Mac Tempas computer program using the following parameters as input: spherical aberration of 1 mm, defocus spread of 8 nm, semiconvergence angle of illumination of 0.55 mrad, and diameter of the objective lens aperture of 7 nm^{-1} .

III. RESULTS AND DISCUSSIONS

The microstructure, chemical composition, and electrostatic potentials of the thin films were investigated by various microscopy techniques. Low-magnification lattice images of samples A (single phase) and B (multilayer film), taken with the incident electron beam parallel to the $[100]$ zone axis of the films, are shown in Figs. 2(a) and 2(b), respectively. Very flat top surfaces and interfaces are seen in both films. The horizontal white arrowheads in the images denote the interfaces between the thin films and the substrates. The epitaxial nature of both films is evident from Fig. 2. One typical selected-area electron diffraction pattern for two samples along the $[100]$ LSCO zone axis was shown in the inset of Fig. 2. It was acquired with an aperture that simultaneously collects scattered electrons coming from the LSCO film and from the LSAO substrate. The diffractogram indicates the following epitaxial orientation relationships between the LSCO film and the LSAO substrate: $[001]_{\text{LSCO}} \parallel [001]_{\text{LSAO}}$ and $[100]_{\text{LSCO}} \parallel [010]_{\text{LSAO}}$. Some distinct splitting of diffraction spots can be detected only along the out-of-the-plane direction, as indicated by the red arrowheads in Figs. 2(a) and 2(b). Based on the tetragonal LSAO lattice with $a = 0.3754 \text{ nm}$ and $c = 1.2635 \text{ nm}$, the image calibration allows us to determine the lattice parameters of the LSCO films: $a = 0.375 \text{ nm}$ and $c = 1.33 \text{ nm}$ in film A versus $a = 0.375 \text{ nm}$ and $c = 1.32 \text{ nm}$ in sample B, both of which are smaller than the original values ($a \approx 0.3775 \text{ nm}$) [18]. The diffractogram observations indicate

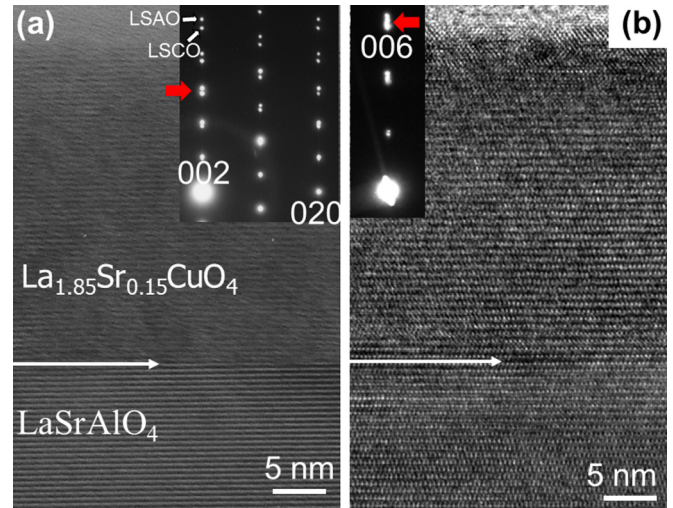


FIG. 2. (Color online) (a), (b) Low-magnification cross-section TEM images of a single-layer LSCO sample A and a multilayer LSCO sample B, respectively. In both samples, sharp and flat top surfaces and interfaces between the films and the substrates are observed. Inset: electron diffraction shows a split peak only in the out-of-plane direction, indicating that both films are epitaxially strained.

that both films are fully strained with very little relaxation. This conclusion was confirmed by HRTEM and STEM (Figs. 3 and 4). The interfacial lattice images of these and other MBE-grown LSCO films show film-substrate interfaces that are atomically sharp over a large area. Few dislocations were detected at the LSCO/LSAO interface due to the small lattice mismatch between the two compounds.

Figure 3(a) shows the $[100]$ lattice fringe image of sample A. Although no misfit dislocations were observed at the interface between LSCO film and LSAO substrate, one kind of heteroepitaxy imperfection was detected: The sequence of atomic layers at the interface between the film and the substrate was found to be different from what one would expect. Image simulation based on the model [the left side in Fig. 3(a)] shows that the stacking sequence at the interface can be described as $(\text{LaSr})\text{O}-(\text{LaSr})\text{O}-\text{AlO}_2-(\text{LaSr})\text{O}-(\text{LaSr})\text{O}-(\text{LaSr})\text{O}-(\text{LaSr})\text{O}-\text{CuO}_2-(\text{LaSr})\text{O}-(\text{LaSr})\text{O}$ [see the red dotted square in Fig. 3(a) and the region between the red dashed line in the structural model], which means that there is an intermediate $(\text{LaSr})_6\text{AlCuO}_{12}$ layer at the interface. Our simulation also shows that in Fig. 3(a), white bright dots in the film and the substrate correspond to the CuO_2 and AlO_2 layers, respectively. The white dots are due to overlapping columns of Cu or Al and oxygen atoms. Using the spacing of AlO_2 - AlO_2 layers along growth direction as the reference, separation of 6.63 \AA between the two nearest CuO_2 planes was obtained directly from the lattice images refinement. The spacing between the last AlO_2 plane and the first CuO_2 plane is 12 \AA . Besides imperfection at the interfaces, inhomogeneous density of atomic columns in CuO_2 layers was also observed in film A. Figures 3(b) and 3(c) are the line scanning profiles of the film and the substrate, respectively. It is clear that the intensity of CuO_2 layer has very large fluctuations, while they are quite small in AlO_2 layers in the substrate. One possibility is that the oxygen vacancies largely occur in the CuO_2 layers.

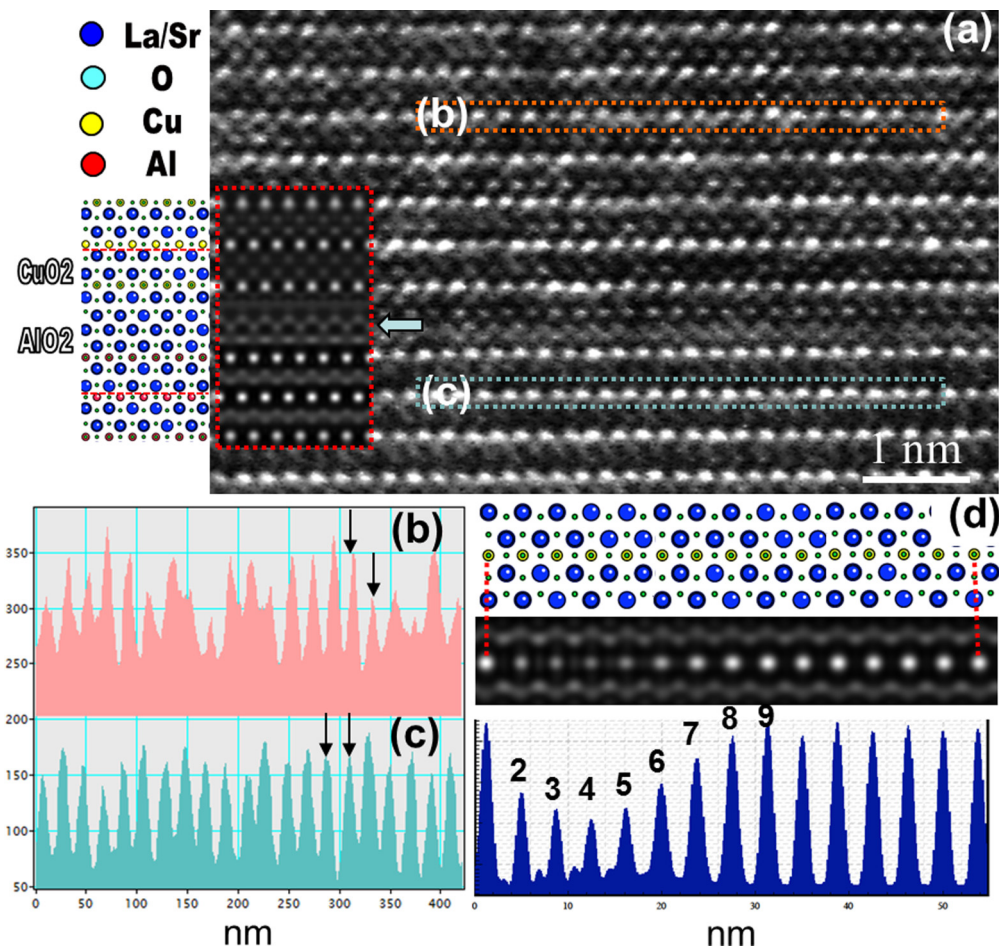


FIG. 3. (Color online) (a) A lattice image of sample A showing formation of an unusual “interface compound”; i.e., a sequence of reconstructed atomic layers that compensate for the polarization discontinuity at the interface. A possible interface model and a simulated image (red dotted square) are shown in the inset. (b), (c) The line profiles from regions in Fig. 3(a) enclosed in red-dotted and blue-dotted rectangles. (d) A model of CuO₂ layer (top) based on the simulated image (middle) and the scanning profile with different oxygen vacancies (numbers 2–9 correspond to the oxygen occupancy from 20–90% in the atomic columns).

As a prerequisite for quantitative measurement of oxygen vacancies, we have investigated the dependence of column image intensity on oxygen occupancy, for example, the fraction of column sites along the view direction occupied by oxygen atoms. Figure 3(d) is a model of the CuO₂ layer with 100% copper occupancy and differing percentages of oxygen occupancy, the simulated images based on our model, and the intensity profile of calculated image. Our model has 15 copper and oxygen overlapping columns for which the occupancy is set to 0.2–0.9 (i.e., 20–90%) for positions 2–9 from left to right; the remaining positions are at 1.0. Aside from oxygen occupancy, the calculated peak intensity of the oxygen columns is dependent on sample thickness and defocus value. Therefore, we simulated images with a range of thickness and defocus values and selected the best one by cross-correlation between experimental and simulated data. We found that the intensity increases linearly with the occupancy when the oxygen vacancy content is greater than 0.3. By comparing the line profiles in Figs. 3(b) and 3(d), the oxygen vacancy concentration in CuO₂ layers should be in the 0.1–0.4 range.

Figure 4(a), the STEM image of the multilayer film (sample B), shows a perfectly coherent interface between the film

and the substrate. The image encompasses one 10-nm-thick film from film/substrate interface, which should include one interface between the sublayers. We cannot see it clearly due to very small differences in composition, or atomic number Z in the projected atom columns, between these two sublayers. However, the average image intensity of the selected region of sublayer 1 in the STEM image is higher than that of sublayer 2, depicted in Fig. 4(b). Sublayer 1 of the film appears about 5 nm thick, in agreement with the MBE growth sequence. In order to investigate the compositional variation of La across the interfaces between the film and the substrate and between the sublayers, a series of high spatial resolution core-loss EELS data in the STEM were collected [32]. Figure 4(c) shows white lines of La $M_{4,5}$ edges across the LSCO/LSAO interface and the sublayer1/sublayer2 interface, corresponding to the positions of the eight colored dots in Fig. 4(a). The EELS data depict that the height of La $M_{4,5}$ peaks of LSAO substrate is about 2.5 arb. units (grid cells), while for sublayers 1 and 2, they are 4 and 3.8 arb. units tall, respectively. This indicates that the difference between the two sublayers can be detected by the line-scanning EELS. In order to further verify whether the sublayer interface is really atomically sharp or not, we

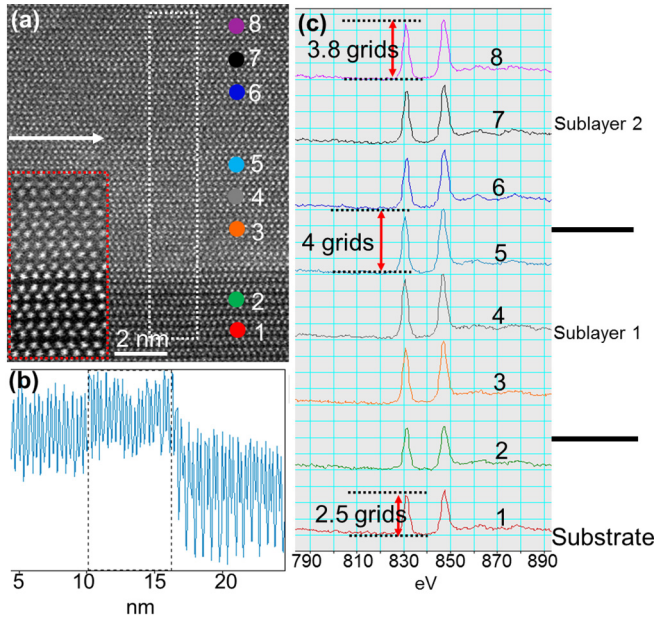


FIG. 4. (Color online) (a) A cross-section STEM image of sample B. The red-dotted square is the enlarged STEM image of the corresponding part. (b) A projected intensity profile from the boxed area in (a). (c) EEL spectra in the energy range from 780 to 890 eV obtained from the eight positions in Fig. 4(a).

investigated the electrostatic potential of each sublayer using off-axis electron holography [33]. Electron holography retrieves the electron-wave phase shift when it passes through the sample that is proportional to the electrostatic potential of the sample. In Fig. 5(a), the bottom part is the ideal case of the potential for each sublayer in the multilayer thin film; the top part is the derivative of the ideal potential of each sublayer, which clearly shows six functionlike peaks for the six interfaces between sublayers. Our electron holography

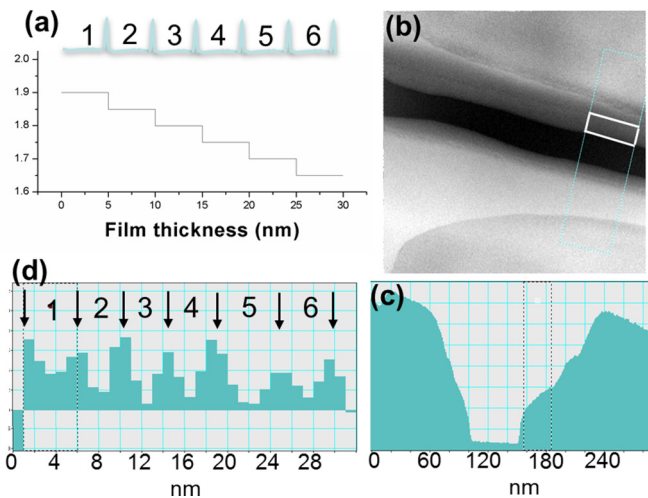


FIG. 5. (Color online) (a) The electrostatic potential distribution of an ideal multilayer thin film and its derivative dI/dx . (b) The reconstructed phase image. (c) The phase shift profile of the multilayer thin film (sample B) in Fig. 5(b). (d) The derivative dI/dx from the boxed region in Fig. 5(c).

experiments agree with the STEM/EELS measurements, further confirming atomically sharp interface between the two sublayers. Figure 5(b) is a reconstructed phase image from electron holograms that includes two pieces of thin film placed together face to face. The dark region (vacuum) separates these two pieces, and each piece contains both the film and the substrate. This phase information reflects the electrostatic potential of the samples; the area outlined by a white box is from the multilayer thin film. Figure 5(c) shows the line-scan of the phase profile of the boxed area in Fig. 5(b), and the dotted rectangle covers the multilayer thin film. The line for the film part is not flat because it includes the phase contribution due to the local thickness variation. It also does not exhibit similar profile as the bottom part in Fig. 5(a) because of the apparatus resolution limit. However, the derivative profile of the potential of the thin film in Fig. 5(d) clearly shows the six peaks, and the spacing between the peaks is around 5–6 nm; these findings match well the MBE growth sequence. These results show that there is a potential jump at the interface between the two sublayers, although they have very small differences in composition. An implication is that the high-quality multilayer film has very sharp interfaces with little or no interdiffusion.

It is well known that both compressive strain and full oxygenation are beneficial to enhance the T_c of LSCO superconductor film [6,8]. Actually, the compressive strain and full oxygenation correlate with each other and are always strengthened or weakened concurrently. This is the exact reason that motivates researchers to achieve structure engineering (e.g., multilayer) to extend compressive strain to all the film regions and full oxygenation in order to enhance the T_c . For monolayer sample A, we found there was an intermediate $(\text{LaSr})_6\text{AlCuO}_{12}$ layer between the LSAO substrate and $\text{La}_{1.85}\text{Sr}_{0.15}\text{CuO}_4$ monolayer film. The interlayer formed to relieve the compressive strain between the substrate, and the film is actually of richer oxygen or poorer copper, compared to LSCO film, and in turn results in the oxygen vacancies in CuO_2 layers of LSCO monolayer film. Thus, the irregular layering sequence interlayer and an abundance of oxygen vacancies near the substrate-film interface made the compressive strain localized at the interface without expanding the compressive strain all over the film (fully strained), thus explaining why T_c was not enhanced in monolayer film system. On the contrary, for multilayer film system, no obvious oxygen vacancies (full oxygenation) can be found, and the interfaces are considerably perfect with little interdiffusion between sublayers (i.e., compressive strain is maintained). Based on these observations, we proved that the compressive strain arising from the slight in-plane lattice difference between LSAO substrate and LSCO film is well extended to all epitaxial film regions, which is believed to be the structure origin of the enhanced T_c in multilayered LSCO film.

The underlying mechanism of the enhancement on the T_c has not been fully understood. The widely accepted strategies to enhance T_c are employing the compressive strain and artificially engineering the multilayer: The compressive strain can enhance the copper-apical-oxygen distance, which scales linearly with T_c [25], while the high-quality multilayer can introduce long-range electrostatic interactions, causing the c axis lattice constant of the top layer to adjust to that of the bottom layer and thus enhancing the T_c of the film [13]. In

the present work, we successfully discovered direct structural evidences for the above two aspects, the so-called structural origin of enhanced T_c . The above obvious difference between multilayer system and monolayer system indicate that the well-maintained compressive strain, full oxygenation, and high-quality multilayers are beneficial to the T_c enhancement, while the interfacial defects (i.e., intermediate layer between substrate and film) and oxygen vacancies have detrimental effects.

IV. CONCLUSION

The microstructure and strain status of LSCO films grown on LSAO substrates by ALL-MBE technique were investigated at atomic scale by TEM combined with HRTEM, STEM,

EELS, and electron holography analysis. Very little or no interdiffusion across the interfaces between the sublayers was observed by STEM, EELS, and electron holography. It was found that the films are fully strained, and this accounts for the enhanced T_c .

ACKNOWLEDGMENTS

Research was supported by the U.S. Department of Energy, Basic Energy Sciences, Materials Sciences and Engineering Division. J.H. thanks M. Schofield and H. Inada for fruitful discussions. This contribution was also supported by the startup of South University of Science and Technology of China from the Shenzhen government and National 1000 Plan for young scientists (J.H.).

-
- [1] J. D. Jorgensen, B. Dabrowski, S. Y. Pei, D. G. Hinks, L. Soderholm, B. Morosin, J. E. Schirber, E. L. Venturini, and D. S. Ginley, *Phys. Rev. B* **38**, 11337 (1988).
- [2] P. G. Radaelli, D. G. Hinks, A. W. Mitchell, B. A. Hunter, J. L. Wagner, B. Dabrowski, K. G. Vandervoort, H. K. Viswanathan, and J. D. Jorgensen, *Phys. Rev. B* **49**, 4163 (1994).
- [3] A. Migliori, W. M. Visscher, S. E. Brown, Z. Fisk, S.-W. Cheong, B. Alten, E. T. Ahrens, K. A. Kubat-Martin, J. D. Maynard, Y. Huang, D. R. Kirk, K. A. Gillis, H. K. Kim, and M. H. W. Chan, *Phys. Rev. B* **41**, 2098 (1990).
- [4] H. Sato and M. Naito, *Physica C* **274**, 221 (1997).
- [5] H. Sato, M. Naito, A. Tsukada, S. Karimoto, and A. Matsuda, *Physica C* **362**, 186 (2001).
- [6] W. D. Si, H. C. Li, and X. X. Xi, *Appl. Phys. Lett.* **74**, 2839 (1999).
- [7] W. D. Si and X. X. Xi, *Appl. Phys. Lett.* **78**, 240 (2001).
- [8] I. Bozovic, G. Logvenov, I. Belca, B. Narimbetov, and I. Sveklo, *Phys. Rev. Lett.* **89**, 107001 (2002).
- [9] M. Abrecht, D. Ariosa, D. Clotta, S. Mitrovic, M. Onellion, X. X. Xi, G. Margaritondo, and D. Pavuna, *Phys. Rev. Lett.* **91**, 057002 (2003).
- [10] H. Oyanagi, A. Tsukada, M. Naito, and N. L. Saini, *Phys. Rev. B* **75**, 024511 (2007).
- [11] D. Ariosa, C. Cancellieri, P. H. Lin, and D. Pavuna, *Appl. Phys. Lett.* **92**, 092506 (2008).
- [12] G. Logvenov, A. Gozar, and I. Bozovic, *Science* **326**, 699 (2009).
- [13] V. Y. Butko, G. Logvenov, N. Bozovic, Z. Radovic, and I. Bozovic, *Adv. Mater.* **21**, 3644 (2009).
- [14] S. Smadici, J. C. T. Lee, S. Wang, P. Abbamonte, G. Logvenov, A. Gozar, C. D. Cavellin, and I. Bozovic, *Phys. Rev. Lett.* **102**, 107004 (2009).
- [15] H. Zhou, Y. Yacoby, V. Y. Butko, G. Logvenov, I. Bozovic, and R. Pindak, *Proc. Natl. Acad. Sci. USA* **107**, 8103 (2010).
- [16] A. T. Bollinger, G. Dubuis, J. Yoon, D. Pavuna, J. Misewich, and I. Bozovic, *Nature* **472**, 458 (2011).
- [17] J. He, R. F. Klie, G. Logvenov, I. Bozovic, and Y. Zhu, *J. Appl. Phys.* **101**, 073906 (2007).
- [18] J. P. Locquet, J. Perret, J. Fompeyrine, E. Machler, J. W. Seo, and G. Van Tendeloo, *Nature* **394**, 453 (1998).
- [19] A. Gozar, G. Logvenov, L. F. Kourkoutis, A. T. Bollinger, L. A. Giannuzzi, D. A. Muller, and I. Bozovic, *Nature* **455**, 782 (2008).
- [20] M. De Llano, M. Lomnitz, and C. Villarreal, *Int. J. Mod. Phys. B* **27**, 1347001 (2013).
- [21] Y. Zhang, P. G. Li, G. F. Wang, Y. Xing, D. S. Wu, J. Q. Shen, M. Lei, and W. H. Tang, *Appl. Phys. Lett.* **102**, 112601 (2013).
- [22] X. Shi, G. Logvenov, A. T. Bollinger, I. Bozovic, C. Panagopoulos, and D. Popovic, *Nat. Mater.* **12**, 47 (2013).
- [23] J. Wu, O. Pelleg, G. Logvenov, A. T. Bollinger, Y. J. Sun, G. S. Boebinger, M. Vanevic, Z. Radovic, and I. Bozovic, *Nat. Mater.* **12**, 877 (2013).
- [24] Y. Ohta, T. Tohyama, and S. Maekawa, *Phys. Rev. B* **43**, 2968 (1991).
- [25] J. A. Slezak, Jinho Lee, M. Wang, K. McElroy, K. Fujita, B. M. Anderson, P. J. Hirschfeld, H. Eisaki, S. Uchida, and J. C. Davis, *Proc. Natl. Acad. Sci. USA* **105**, 3203 (2008).
- [26] O. Yuli, I. Asulin, O. Millo, D. Orgad, L. Iomin, and G. Koren, *Phys. Rev. Lett.* **101**, 057005 (2008).
- [27] G. Koren and O. Millo, *Phys. Rev. B* **80**, 054507 (2009).
- [28] N. Reyren, S. Thiel, A. D. Caviglia, L. Fitting Kourkoutis, G. Hammerl, C. Richter, C. W. Schneider, T. Kopp, A.-S. Rüetschi, D. Jaccard, M. Gabay, D. A. Muller, J.-M. Triscone, and J. Mannhart, *Science* **317**, 1196 (2007).
- [29] J. Pereiro, A. T. Bollinger, G. Logvenov, A. Gozar, C. Panagopoulos, and I. Bozovic, *Phil. Trans. R. Soc. A* **370**, 4890 (2012).
- [30] J. N. Eckstein, I. Bozovic, and G. F. Virshup, *MRS Bull.* **19**, 44 (1994).
- [31] I. Bozovic, *IEEE Trans. Appl. Supercond.* **11**, 2686 (2001).
- [32] R. F. Egerton, *Electron Energy-Loss Spectroscopy in the Electron Microscope*, 2nd ed. (Plenum, New York, 1996).
- [33] M. A. Schofield, L. Wu, and Y. Zhu, *Phys. Rev. B* **67**, 224512 (2003).